Enhancement of proton energy by polarization switch in laser acceleration of multi-ion foils

Tung-Chang Liu, Xi Shao, Chuan-Sheng Liu, Bengt Eliasson, Jyhpyng Wang, and Shih-Hung Chen

Citation: Physics of Plasmas (1994-present) **20**, 103112 (2013); doi: 10.1063/1.4826510
View online: http://dx.doi.org/10.1063/1.4826510
View Table of Contents: http://scitation.aip.org/content/aip/journal/pop/20/10?ver=pdfcov
Published by the AIP Publishing

Enhancement of proton energy by polarization switch in laser acceleration of multi-ion foils

Tung-Chang Liu,[1,a)] Xi Shao,[1] Chuan-Sheng Liu,[1] Bengt Eliasson,[1,2] Jyhpyng Wang,[3,4] and Shih-Hung Chen[4]
[1]*Department of Physics, University of Maryland, College Park, Maryland 20742, USA*
[2]*Department of Physics, University of Strathclyde, Glasgow G4 0NG, Scotland, United Kingdom*
[3]*Institute of Atomic and Molecular Sciences, Academia Sinica, Taipei 10617, Taiwan*
[4]*Department of Physics, National Central University, Taoyuan 32001, Taiwan*

(Received 13 June 2013; accepted 9 October 2013; published online 18 October 2013)

We present a scheme to significantly increase the energy of quasi-monoenergetic protons accelerated by a laser beam without increasing the input power. This improvement is accomplished by first irradiating the foil several wave periods with circular polarization and then switching the laser to linear polarization. The polarization switch increases the electron temperature and thereby moves more electrons ahead of the proton layer, resulting in a space charge electric field pushing the protons forwards. The scaling of the proton energy evolution with respect to the switching time is studied, and an optimal switching time is obtained. The proton energy for the case with optimal switching time can reach about 80 MeV with an input laser power of 70 TW, an improvement of more than 30% compared to the case without polarization switch. © *2013 AIP Publishing LLC*. [http://dx.doi.org/10.1063/1.4826510]

I. INTRODUCTION

Recently, there has been an active research on advancing laser particle acceleration schemes for medical applications such as proton cancer therapy, where the proton energy is required to be tunable in the range of 50–250 MeV and to be monoenergetic in order to target the tumor location accurately. In this regard, a compact laser-driven proton accelerator is an attractive alternative compared to traditional accelerators since the electric fields for particle acceleration can reach the order of tens of GV per cm, allowing large reduction in the system size. There are mainly two mechanisms for proton acceleration by laser irradiation of a foil, target normal sheath acceleration (TNSA) and radiation pressure acceleration (RPA). In TNSA, solid targets with thicknesses ranging from a few to several tens of laser wavelengths are used. The intense laser heats the electrons on one side of the foil, and the laser-heated electrons form a hot sheath on the opposite side of the foil, which accelerates impurities of protons to multi-tens MeV energies.[1–10] However, the resulting ion energy spectra are in most cases broad and only few protons reach the maximum energy, which is less suitable for applications requiring monoenergetic protons.

The scheme of laser RPA of quasi-monoenergetic protons has been actively studied in theory and simulations[11–19] and experiments.[20,21] In RPA, or equivalently "light sail," high intensity circularly polarized laser light with a high contrast ratio accelerates nearly the whole thin foil by the radiation pressure. In an accelerating frame co-moving with the proton layer, protons are subject to both the electric force of the electron layer accelerating them forward and the inertial force pulling them back. The balance of these two opposing forces forms a trap for the ions in real and phase spaces. On the other hand, the electrons are trapped by a combination of the laser ponderomotive force and the electric force due to the ions. These stably trapped protons and electron layers form a self-organized double layer.[17] This is a more efficient acceleration process for producing high energy monoenergetic protons, suitable for many applications requiring that the accelerated protons have good beam quality and a narrow energy spectrum. However, previous works demonstrated with two-dimensional (2D) particle-in-cell (PIC) simulations[16,18,22–24] that the Rayleigh-Taylor instability (RTI) limits the acceleration achieved by RPA and rapidly broadens the proton beam's energy spectrum. For RPA of thin-foil targets of one species, the energy scaling study with PIC simulation[18] indicates that petawatt power laser is needed to obtain ~200 MeV quasi-monoenergetic protons with energy spread within 20% of the peak flux energy, which may make the laser proton acceleration scheme less attractive for commercial practical applications, as it is difficult to build a petawatt laser, and the laser also produces strong radiation that is difficult to shield.[25,26]

However, by using a thin composite multi-ion proton-carbon foil, researches have shown that the energy can be further increased.[27–32] In particular, our recent work[32] found that higher proton energy is mainly resulting from two different stages of acceleration. First, there is an RPA stage, in which the heavier carbon ions are less accelerated and left behind the lighter protons, forming a triple layer system. After the electron layer is disrupted by the RTI, the shielded Coulomb repulsion (SCR) stage takes place, in which the proton layer continues to be pushed by the carbon ion layer behind and is further accelerated. The Coulomb repulsion of the proton layer by the carbon layer can help remedy the RTI and further accelerate the protons. Using a laser beam with 70 TW power to irradiate a carbon-proton target with 10%

[a)]E-mail: tcliu@umd.edu

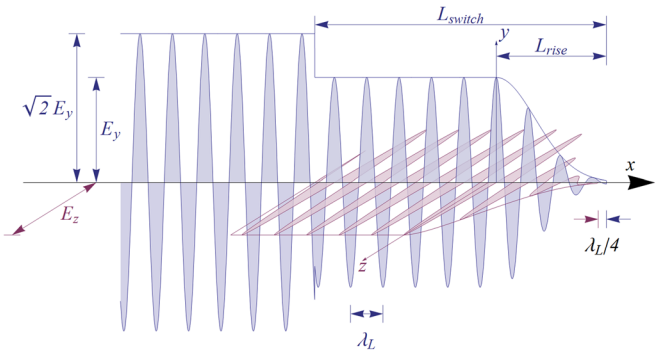

FIG. 1. The profile along the $x-$ axis of the injected laser electric field. The parameter L_{switch} in the figure is denoted as L_S in the text.

protons, we can achieve a quasi-monoenergetic proton beam with 60 MeV of energy, which is several times the energy obtainable from a pure hydrogen foil.

In this paper, we present a scheme based on the SCR to further boost the energy of the monoenergetic protons without increasing the input laser power. It has been shown that circularly polarized waves can accelerate the protons monoenergetically by suppressing the oscillatory motion of electrons, whereas linear polarization waves broaden the electrons more rapidly with higher temperature.[33–35] In our scheme, we combine the advantages of these two by switching the laser from circular to linear polarization after that the RPA has fully separated the protons from carbon ions, and the electron temperature is significantly increased due to the oscillatory ponderomotive force by the linearly polarized laser, allowing larger amount of electrons to be distributed in front of the proton layer and to provide a force pulling the proton layer forward. Our 2D PIC simulations show that 80 MeV of proton energy can be achieved using the polarization switch, an improvement of more than 30% compared to the previous result of 60 MeV using only circular polarization.

II. SIMULATION SETUP

In order to demonstrate the acceleration scheme with polarization switch, we employ 2D PIC simulations and analyze the dynamics of the macro-particles to compare the differences among different switching conditions. The simulation domain is $-30 \le x/\lambda_L \le 70$ and $-15 \le y/\lambda_L \le 15$, and the grid size is $\lambda_L/100$ in both the x and y dimensions, where $\lambda_L = 1.0\,\mu$m is the laser wavelength. The boundary conditions are absorbing at all boundaries for particles and fields, and the laser electromagnetic wave is injected at the $-x$ boundary. The foil, consisting of 90% carbon and 10% hydrogen, is initially located at $0 \le x \le l_0$ and is resolved by 49 macro-particles of each species per cell with initial thickness $l_0 = 0.2\lambda_L$ and electron density $n_{e0} = 8.3n_{cr}$. Here, $n_{cr} = \varepsilon_0 m_e \omega_L^2/e^2$ is the critical density, where m_e is the mass of an electron, e is the elementary charge, ε_0 is the vacuum permittivity, and ω_L is the laser angular frequency. The amplitude of the incident laser beam has a Gaussian profile in the transverse direction with spot size, defined as the diameter at e^{-2} of the peak intensity, being $16\lambda_L$. The spatial profile along the x-axis is shown in Figure 1. The profile of the input laser is a combination of an $L_R = 3\lambda_L$ Gaussian raising,

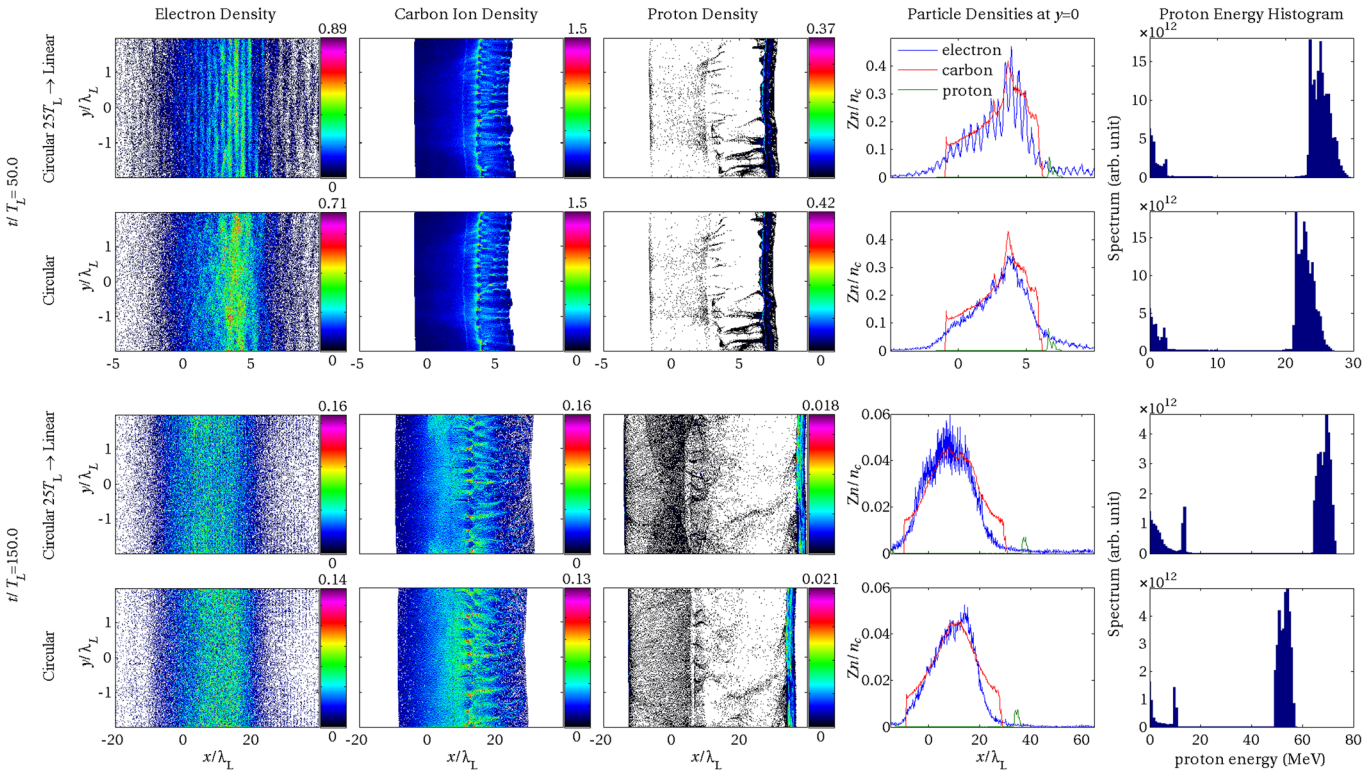

FIG. 2. Comparison of particle densities and proton energy between cases with and without polarization switch. The upper half panels show simulation data at $t = 50T_L$, and the lower half ones at $t = 150T_L$. The first and third rows show cases with laser switching from circular to linear polarization with $L_S = 25\lambda_L$, and the second and fourth rows show cases one with circular polarization. The columns from left to right are, respectively, the data of electron, carbon ion, and proton density distribution, all particle densities at the center axis and proton energy histogram.

continuous circular polarized wave until L_S, and then linear polarized wave thereafter. The normalized laser amplitude is $a_0 = eE_{y,z}/m_e\omega_L c = 5$, corresponding to 70 TW input power. The total power of the laser beam is the same before and after the switch, and therefore the amplitude after the switch is increased by a factor of $\sqrt{2}$. The switching parameter L_S is varied for different sets of simulations.

III. SIMULATION RESULTS

We compare the simulation results for the cases with polarization switch at $L_S = 25\lambda_L$ and without polarization switch, as shown in Figure 2. The general acceleration mechanisms for both cases are similar. A triple layer consisting of proton, electron, and carbon is formed, and the proton layer continues to be accelerated by Coulomb repulsion from the net charge of carbon and electron layers after that the RTI has disrupted the electron layer. On the other hand, the density distributions of electrons, which shield most of carbon charge's contribution to Coulomb repulsion, are very different between the two cases. At the earlier stage $t = 50T_L$ (upper half panels), we can visibly observe the wave-like structure in the longitudinal direction of the electron distribution from the foil irradiated by linear polarized laser beam (the first row), whereas the structure is smoother in the one with circular polarization (the second row). The linearly polarized laser beam conveys more energy to electrons due to both the oscillatory electric field in transverse direction and the enhanced peak amplitude, resulting in a distribution with more energetic electrons capable of staying in front of the proton layer instead of being pulled back by the carbon layer, as shown in the fourth column of Figure 2. Therefore, the shielding effect of Coulomb repulsion due to electrons trapped in the carbon layer is also strongly reduced, resulting in an increase in the proton acceleration efficiency as shown in the last column of Figure 2.

At a later stage at $t = 150T_L$ (lower half panels of Figure 2), a more clear improvement in the obtainable proton energy can be seen. We observe in the electron density distribution that the two key features of the case with a linear polarized beam (the third row of Figure 2), which are the oscillatory motion and ahead-of-proton distribution of electrons, last for a significant time. This heavy-tail distribution then provides a larger electrostatic force pushing the protons and resulting in a substantial improvement of the proton energy to 68 MeV as shown in the last column of Figure 2. In comparison, a proton energy of only 55 MeV is achieved in the case without switch (the fourth row of Figure 2).

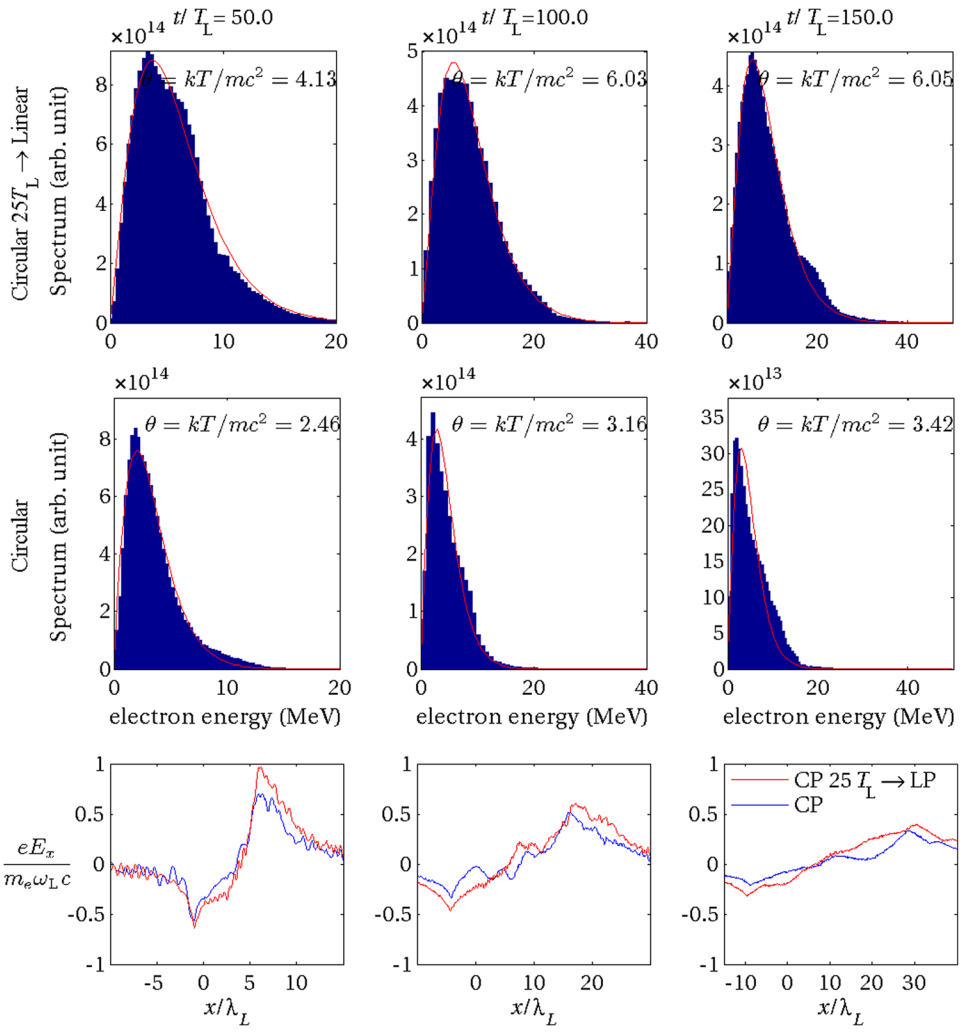

FIG. 3. The electron energy histogram in the center-of-mass frame (the first two rows) and the electrostatic field (the third row) for the cases with and without polarization switch. The first and second rows show histograms with and without polarization switch, respectively. The red curves in the first two rows are fittings of relativistic Maxwellian distributions with temperatures shown on the plots. The third row is the normalized electric fields in x direction, where the red curves are the longitudinal electric field with polarization switch, and the blue curves without polarization switch. The data are shown at $t = 50T_L$, $100T_L$, and $150T_L$ from the first to the third column, respectively.

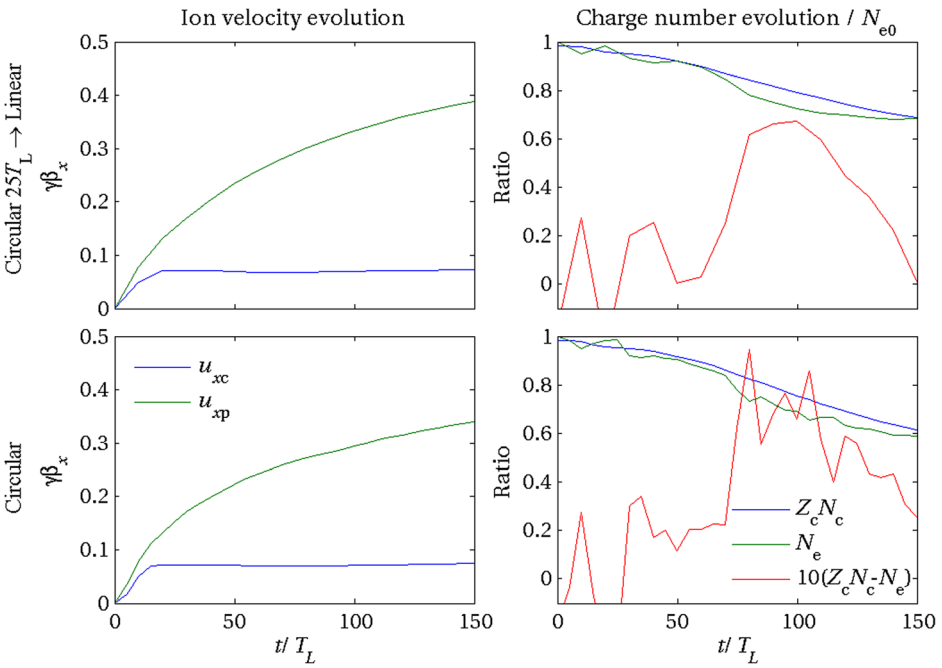

FIG. 4. The evolution of particle momentum (the first column) and number (the second column) with and without polarization switch. The upper and lower rows are the switching and non-switching cases, respectively. In the figure of particle number, the charge difference (red line) is scaled up ten times to feature the comparison between cases.

IV. DATA ANALYSIS

To explain the enhanced proton energy resulting from polarization switch, we further analyze the particle and field distribution data in detail. It has already been shown[32] that during the process of SCR, the proton energy evolution can be approximated by a simple one-dimensional model, assuming the proton layer as a test charge, the electron distribution as Maxwellian, and the carbon layer as moving with constant velocity. The equation of motion of the proton layer is[32]

$$\begin{cases} \dfrac{\mathrm{d}x_\mathrm{p}}{\mathrm{d}t} = v_\mathrm{p}, \\ \dfrac{\mathrm{d}(\gamma_\mathrm{p} v_\mathrm{p})}{\mathrm{d}t} = \dfrac{eE_x}{m_\mathrm{p}} = \dfrac{e\sigma_\mathrm{net}}{2\varepsilon_0 m_\mathrm{p}} \coth \dfrac{(x_\mathrm{p} - v_\mathrm{C} t) e\sigma_\mathrm{net}}{4\varepsilon_0 k_\mathrm{B} T_\mathrm{e}}, \end{cases} \tag{1}$$

where x_p, v_p, and γ_p are, respectively, the position, velocity, and relativistic gamma factor of the proton layer, v_C is the velocity of the carbon ion layer, e and m_p are, respectively, the charge and mass of a proton, ε_0 is the vacuum electric permittivity, k_B is Boltzmann's constant, E_x is the longitudinal electric field at x_p, T_e is the electron temperature, and σ_net is the net surface charge density.

Equation (1) shows that there are mainly three parameters deciding the acceleration of the proton layer: T_e, v_C, and σ_net. In Figure 3, we demonstrate the fitting of electron energy histogram in the center-of-mass frame with relativistic Maxwellian distribution in the first two rows, one with polarization switch and the other without. It can be seen that not only do they fit well with Maxwellian distributions, which satisfies the assumption of the model, but also the temperature of the case with polarization switch is also significantly greater, indicating a greater electric field and acceleration (the third row of Figure 3). The other two parameters v_C and σ_net, on the other hand, do not change considerably regarding the switch, as presented in Figure 4, implying that the remarkable improvement of proton velocity, which is also shown in the first column of Figure 4, results mainly from the wider distribution of hotter electrons.

To demonstrate the agreement between the simulation result and the theoretical prediction in 1D model, we plot the evolution of the average momentum of proton in Figure 5. The initial conditions we imposed in the theory are $k_\mathrm{B}T_\mathrm{e}/m_\mathrm{e}c^2 = 6.0$, $\sigma_\mathrm{net}/\sigma_\mathrm{e0} = 0.07$, $\gamma_\mathrm{p0}v_\mathrm{p0} = 0.23c$, and $x_\mathrm{p0} = 1.7\lambda_\mathrm{L}$. This 1D model successfully describes the proton energy evolution, while the distance between the proton and

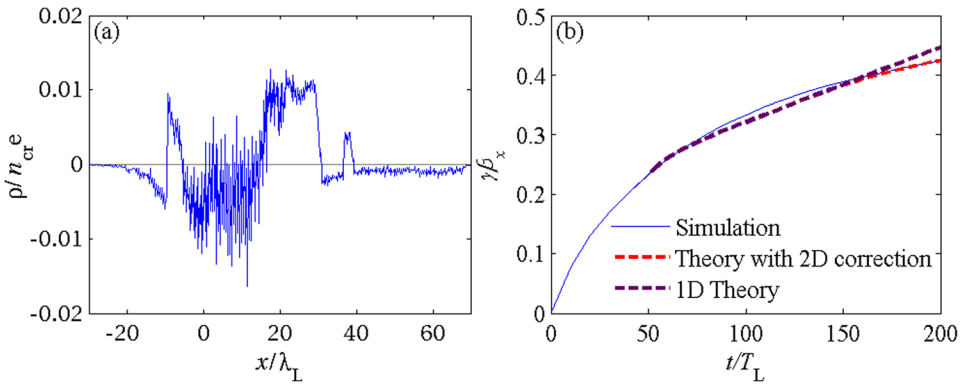

FIG. 5. (a) Net charge density distribution at the center axis at $t = 150T_\mathrm{L}$. (b) Comparison between theory and simulation in momentum evolution of quasi-monoenergetic protons with switching time being 25 wave periods. The dashed lines are the theoretical prediction with normalized temperature 6 and net charge being 7% of the initial value. The purple one is the original 1D model prediction, and the red one is calculated using the 2D equation of motion while $x_\mathrm{p} - v_\mathrm{C}t > 20\lambda_\mathrm{L}$.

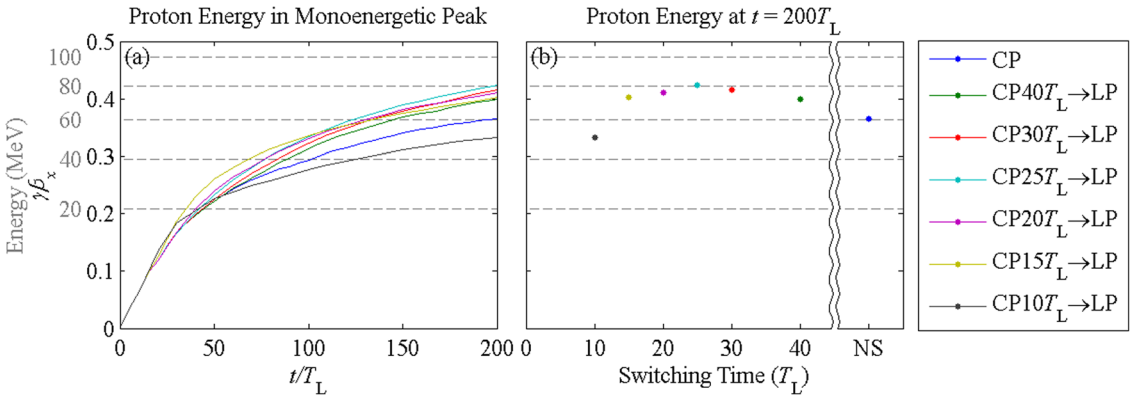

FIG. 6. (a) Momentum evolution of quasi-monoenergetic protons with switching time scaling from 10 to 40 wave periods. The dashed lines indicate the equivalent energy scale. (b) The proton energy at $t = 200T_L$ for different switching times, where NS denotes the non-switching case. The optimal time of switching is $t_S = 25T_L$.

carbon layers is moderate compared to the laser spot size. However, the momentum evolution trend for large separation, which is comparable to the spot size as shown in Figure 5(a) when $t = 150T_L$, is then different. We apply a minor modification to consider the Coulomb potential in 2D situation when the separation between the proton and carbon layers is large and includes the derivation in Appendix. The comparison of momentum evolution between theoretical predictions and the simulation result is shown in Figure 5(b).

V. SCALING

Since we have demonstrated that performing polarization switch from circular to linear polarization can increase the electron temperature, resulting in larger portion of electrons staying ahead of the proton layer, and consequently generate quasi-monoenergetic protons with higher energy, it is of interest whether there exists an optimal switching time. To explore the relationship between the switching time and the obtainable monoenergy, we perform simulations by varying the switching time by $5T_L$ in each simulation, and display the result in Figure 6. The resultant proton quasi-monoenergy is maximized when the laser polarization is switched from circular to linear $t_S = 25T_L$ after hitting the foil, demonstrating the existence of optimal switching time.

The reason for that $t_S = 25T_L$ is an optimal switching time, which is mainly the balance between the effectiveness of SCR and the complete separation between carbon ions and protons due to the RPA. It is clear that switching to linear polarization can increase the acceleration efficiency of SCR, and one may consider to switch it as soon as possible. However, a principal presumption of SCR is full separation between the carbon ions and protons, which is primarily based on the uneven acceleration of RPA on the charges with different charge-to-mass ratios. Therefore, if the laser polarization is switched before full separation between protons and carbon ions occurs, the efficiency of SCR is reduced and the protons spread out in energy. In Figure 6, we can conclude that the proton energy with an optimal switching time can reach about 30% more than the one achieved with a purely circularly polarized case at $t = 200T_L$, and that the RPA induced charge separation phase is crucial in this mechanism as the proton energy obtained with complete linear polarization is even worse than the one with complete circular polarization.

VI. CONCLUSION

In summary, we demonstrated through 2D PIC simulations that polarization switch can increase the energy of quasi-monoenergetic proton by 30% without increasing the input power, indicating that the efficiency is increased by 30% as well. The main reason for such an improvement is due to larger proportion of electrons in front of the proton layer resulting from higher energy, making those electrons pull the protons forward instead of backward. The optimal time to switch from circular to linear polarization with typical input parameters $a_0 = 5$, $l_0 = 0.2\lambda_L$, $n_{e0} = 8.3n_{cr}$, and n_{C0}: $n_{p0} = 9:1$ for a 70 TW laser is $25T_L$, a time period required for the RPA to completely separate the proton layer from the carbon ion layer. Numerically, we can generate a quasi-monoenergetic proton beam of 80 MeV by a laser beam with moderate power of 70 TW, which is promising for future applications.

ACKNOWLEDGMENTS

This work was supported by US DoE Grant No. DE-SC0008391. We would like to acknowledge the National Center for High-Performance Computing in providing resources under the national project "Taiwan Knowledge Innovation National Grid."

APPENDIX: 2D MODIFICATION OF THE EQUATION OF MOTION

Previously, we calculated the equation of motion using 1D Poison equation. However, as the separation between the protons and the carbon ions becomes longer and longer, the consequence that electrostatic field converges to a non-zero constant in the 1D model is no longer valid, and therefore considering the equation of motion in 2D geometry becomes necessary. When distance is comparable with or greater than the spot size, we then neglect the insignificant portion of

electrons moving to the other side of proton layer and assume simply that the net charge behind the proton layer is a constant and can be approximated as a uniformly charged cylinder with its axis aligned with z-direction. Therefore, the electric field can be simply written as

$$E_x = \frac{e}{2\pi\varepsilon_0(x_p - v_C t)} \int_R n_{net} d\sigma, \tag{A1}$$

where R denotes a limited region behind the proton layer where carbon ion is the dominant species. When $t = 150T_L$, the time when $x_p - v_C t$ becomes greater than the threshold distance $x_{th} = 20\lambda_L$, which we choose to be slightly greater than the spot size, and the longitudinal dimension of region R is about 15 wavelength, as shown in Figure 5(a). The y-direction in the integration is decided from the initial condition $E_{x,1D} = E_{x,2D}$ as a continuous connection between these two models. We can, therefore, obtain the equation of motion similar to Eq. (1), but substitute the acceleration term as

$$\frac{d(\gamma_p v_p)}{dt} = \frac{eE_x}{m_p} = \begin{cases} \dfrac{e\sigma_{net}}{2\varepsilon_0 m_p} \coth \dfrac{(x_p - v_C t) e\sigma_{net}}{4\varepsilon_0 k_B T_e}, & x_p - v_C t < x_{th} \\ \dfrac{e\sigma_{net}}{2\varepsilon_0 m_p} \dfrac{x_{th}}{x_p - v_C t} \coth \dfrac{x_{th} e\sigma_{net}}{4\varepsilon_0 k_B T_e}, & x_p - v_C t \geq x_{th}. \end{cases} \tag{A2}$$

The correction successfully resolves the issue that the acceleration does not approach zero as distance increases and provides a more reasonable result compared with simulation. Furthermore, in real 3D condition, we should consider the electric field as

$$E_x = \frac{e}{4\pi\varepsilon_0(x_p - v_C t)^2} \int_R n_{net} dV, \tag{A3}$$

which decreases even faster with increasing distance.

[1]S. C. Wilks, A. B. Langdon, T. E. Cowan, M. Roth, M. Singh, S. Hatchett, M. H. Key, D. Pennington, A. MacKinnon, and R. A. Snavely, Phys. Plasmas **8**, 542 (2001).
[2]A. Pukhov, Phys. Rev. Lett. **86**, 3562 (2001).
[3]H. Schwoerer, S. Pfotenhauer, O. Jäckel, K.-U. Amthor, B. Liesfeld, W. Ziegler, R. Sauerbrey, K. W. D. Ledingham, and T. Esirkepov, Nature **439**, 445 (2006).
[4]B. M. Hegelich, B. J. Albright, J. Cobble, K. Flippo, S. Letzring, M. Paffett, H. Ruhl, J. Schreiber, R. K. Schulze, and J. C. Fernández, Nature **439**, 441 (2006).
[5]S. Ter-Avetisyan, M. Schnürer, P. V. Nickles, M. Kalashnikov, E. Risse, T. Sokollik, W. Sandner, A. Andreev, and V. Tikhonchuk, Phys. Rev. Lett. **96**, 145006 (2006).
[6]J. Fuchs, C. A. Cecchetti, M. Borghesi, T. Grismayer, E. d'Humières, P. Antici, S. Atzeni, P. Mora, A. Pipahl, L. Romagnani, A. Schiavi, Y. Sentoku, T. Toncian, P. Audebert, and O. Willi, Phys. Rev. Lett. **99**, 015002 (2007).
[7]P. Mora, AIP Conf. Proc. **920**, 98 (2007).
[8]L. Yin, B. J. Albright, B. M. Hegelich, K. J. Bowers, K. A. Flippo, T. J. T. Kwan, and J. C. Fernández, Phys. Plasmas **14**, 056706 (2007).
[9]L. Robson, P. T. Simpson, R. J. Clarke, K. W. D. Ledingham, F. Lindau, O. Lundh, T. McCanny, P. Mora, D. Neely, C.-G. Wahlström, M. Zepf, and P. McKenna, Nat. Phys. **3**, 58 (2007).
[10]L. Yin, B. J. Albright, K. J. Bowers, D. Jung, J. C. Fernández, and B. M. Hegelich, Phys. Rev. Lett. **107**, 045003 (2011).
[11]T. Esirkepov, M. Borghesi, S. V. Bulanov, G. Mourou, and T. Tajima, Phys. Rev. Lett. **92**, 175003 (2004).
[12]X. Q. Yan, C. Lin, Z. M. Sheng, Z. Y. Guo, B. C. Liu, Y. R. Lu, J. X. Fang, and J. E. Chen, Phys. Rev. Lett. **100**, 135003 (2008).
[13]C. S. Liu, V. K. Tripathi, and X. Shao, AIP Conf. Proc. **1061**, 246 (2008).
[14]O. Klimo, J. Psikal, J. Limpouch, and V. T. Tikhonchuk, Phys. Rev. ST Accel. Beams **11**, 031301 (2008).
[15]V. K. Tripathi, C. S. Liu, X. Shao, B. Eliasson, and R. Z. Sagdeev, Plasma Phys. Controlled Fusion **51**, 024014 (2009).
[16]A. P. L. Robinson, M. Zepf, S. Kar, R. G. Evans, and C. Bellei, New J. Phys. **10**, 013021 (2008).
[17]B. Eliasson, C. S. Liu, X. Shao, R. Z. Sagdeev, and P. K. Shukla, New J. Phys. **11**, 073006 (2009).
[18]T.-C. Liu, X. Shao, C.-S. Liu, J.-J. Su, B. Eliasson, V. Tripathi, G. Dudnikova, and R. Z. Sagdeev, Phys. Plasmas **18**, 123105 (2011).
[19]M.-Q. He, X. Shao, C.-S. Liu, T.-C. Liu, J.-J. Su, G. Dudnikova, R. Z. Sagdeev, and Z.-M. Sheng, Phys. Plasmas **19**, 073116 (2012).
[20]A. Henig, S. Steinke, M. Schnürer, T. Sokollik, R. Hörlein, D. Kiefer, D. Jung, J. Schreiber, B. M. Hegelich, X. Q. Yan, J. Meyer-ter-Vehn, T. Tajima, P. V. Nickles, W. Sandner, and D. Habs, Phys. Rev. Lett. **103**, 245003 (2009).
[21]D. Jung, L. Yin, B. J. Albright, D. C. Gautier, R. Hörlein, D. Kiefer, A. Henig, R. Johnson, S. Letzring, S. Palaniyappan, R. Shah, T. Shimada, X. Q. Yan, K. J. Bowers, T. Tajima, J. C. Fernández, D. Habs, and B. M. Hegelich, Phys. Rev. Lett. **107**, 115002 (2011).
[22]F. Pegoraro and S. V. Bulanov, Phys. Rev. Lett. **99**, 065002 (2007).
[23]C. S. Liu, X. Shao, B. Eliasson, T. C. Liu, G. Dudnikova, and R. Z. Sagdeev, AIP Conf. Proc. **1320**, 104 (2011).
[24]C. A. J. Palmer, J. Schreiber, S. R. Nagel, N. P. Dover, C. Bellei, F. N. Beg, S. Bott, R. J. Clarke, A. E. Dangor, S. M. Hassan, P. Hilz, D. Jung, S. Kneip, S. P. D. Mangles, K. L. Lancaster, A. Rehman, A. P. L. Robinson, C. Spindloe, J. Szerypo, M. Tatarakis, M. Yeung, M. Zepf, and Z. Najmudin, Phys. Rev. Lett. **108**, 225002 (2012).
[25]C. Joshi, Phys. Plasmas **14**, 055501 (2007).
[26]E. Esarey, P. Sprangle, J. Krall, and A. Ting, IEEE Trans. Plasma Sci. **24**, 252 (1996).
[27]S. S. Bulanov, A. Brantov, V. Y. Bychenkov, V. Chvykov, G. Kalinchenko, T. Matsuoka, P. Rousseau, S. Reed, V. Yanovsky, D. W. Litzenberg, K. Krushelnick, and A. Maksimchuk, Phys. Rev. E **78**, 026412 (2008).
[28]T.-P. Yu, A. Pukhov, G. Shvets, and M. Chen, Phys. Rev. Lett. **105**, 065002 (2010).
[29]B. Qiao, M. Zepf, M. Borghesi, B. Dromey, M. Geissler, A. Karmakar, and P. Gibbon, Phys. Rev. Lett. **105**, 155002 (2010).
[30]T. P. Yu, A. Pukhov, G. Shvets, M. Chen, T. H. Ratliff, S. A. Yi, and V. Khudik, Phys. Plasmas **18**, 043110 (2011).
[31]K. H. Pae, I. W. Choi, and J. Lee, Laser Part. Beams **29**, 11 (2011).
[32]T.-C. Liu, X. Shao, C.-S. Liu, M. He, B. Eliasson, V. Tripathi, J.-J. Su, J. Wang, and S.-H. Chen, New J. Phys. **15**, 025026 (2013).
[33]A. Macchi, F. Cattani, T. V. Liseykina, and F. Cornolti, Phys. Rev. Lett. **94**, 165003 (2005).
[34]T. V. Liseikina and A. Macchi, Appl. Phys. Lett. **91**, 171502 (2007).
[35]S. G. Rykovanov, J. Schreiber, J. Meyer-ter-Vehn, C. Bellei, A. Henig, H. C. Wu, and M. Geissler, New J. Phys. **10**, 113005 (2008).